

# Analysis of Spliceosome Dynamics by Maximum Likelihood Fitting of Dwell Time Distributions

## Authors:

5 Harpreet Kaur<sup>1</sup>, Fatemehsadat Jamalidinan<sup>1</sup>, Samson G.F. Condon<sup>1</sup>, Alessandro Senes<sup>1</sup>,  
6 and Aaron A. Hoskins<sup>1\*</sup>

## Affiliations:

8 1. Department of Biochemistry, 433 Babcock Dr., University of Wisconsin-Madison,  
9 Madison, WI 53706 USA

## 10 Corresponding Author:

11 Aaron A. Hoskins, [ahoskins@wisc.edu](mailto:ahoskins@wisc.edu), 608-890-3101

13 **Contents**

- 14 1. Introduction
- 15 2. Example Data and Initial Analysis
  - 16 2.1. RNA Binding Dynamics of a Yeast Splicing Factor
  - 17 2.2. Obtaining a List of Dwell Times from Movies of Single Molecules
  - 18 2.3. Plotting the Single-Molecule Data as a Distribution of Dwell Times
- 19 3. Methods for Fitting Distributions of Dwell Times
  - 20 3.1. Obtaining the Fit Parameters and Associated Errors
  - 21 3.2. Determining the Goodness of the Fit
  - 22 3.3. Comparison Between Maximum Likelihood and Least Square Fitting
- 23 4. Use of AGATHA Software for ML Fitting
  - 24 4.1. Plotting Histograms
  - 25 4.2. Instructions for Using the Plotting Histogram Program
- 26 5. Conclusion
- 27 Acknowledgements
- 28 References

29 **Abstract**

30 Colocalization single-molecule methods can provide a wealth of information  
31 concerning the ordering and dynamics of biomolecule assembly. These have been used  
32 extensively to study the pathways of spliceosome assembly *in vitro*. **Key to these**  
33 **experiments is the measurement of binding times—either the dwell times of a multi-**  
34 **molecular interaction or times in between binding events.** By analyzing hundreds of **these**  
35 times, many new insights into the kinetic pathways governing spliceosome assembly  
36 have been obtained. Collections of **binding** times are often plotted as histograms and can  
37 be fit to kinetic models using a variety of methods. Here, we describe the use of maximum  
38 likelihood methods to fit dwell time distributions without binning. In addition, we discuss  
39 several aspects of analyzing these distributions with histograms and pitfalls that can be  
40 encountered if improperly binned histograms are used. We have automated several  
41 aspects of maximum likelihood fitting of dwell time distributions in the AGATHA software  
42 package.

43 **Keywords**

44 single-molecule, fluorescence, spliceosome, dynamics, software, fitting

45 **Highlights**

46

- 47 • Single-molecule methods can measure discrete binding events between  
individual biomolecules

48

- 49 • Maximum likelihood fitting of unbinned binding data can be used to determine  
kinetic parameters

50

- 51 • AGATHA software automates many time-consuming steps in data fitting and  
histogram analysis

52 **1. Introduction**

53       The spliceosome is an extremely complex and highly dynamic molecular machine  
54    found in eukaryotes [1]. It carries out precursor mRNA (pre-mRNA) splicing by concerted  
55    removal of intronic sequences and ligation of the flanking exons. The splicing process  
56    requires the coordinated action of five small nuclear ribonucleoprotein particles (snRNPs):  
57    U1, U2, U4, U5 and U6. Each snRNP contains a uridine-rich small nuclear RNA (U  
58    snRNA) and several snRNP-specific proteins [2]. In addition to large-scale conformational  
59    rearrangements of the snRNPs, numerous other splicing factors assemble, rearrange  
60    and/or dissociate from the spliceosome during each step of splicing [2-5]. Single-  
61    molecule fluorescence microscopy methods such as single-molecule FRET (smFRET)  
62    and colocalization single-molecule spectroscopy (CoSMoS) have revealed the transient  
63    behaviors of the spliceosome that are often obscured by ensemble techniques. In fact,  
64    splicing was first discovered through single-molecule imaging of RNA/DNA hybrids using  
65    electron microscopy [6, 7]. Recent high resolution cryo-EM structures have revealed the  
66    overall structure, and detailed inner-workings of the several key states of the spliceosome  
67    [4-6]. The structural rearrangements observed in these different states have  
68    revolutionized our understanding of splicing mechanism as well as validated key single-  
69    molecule results concerning juxtaposition of the sites of splicing chemistry prior to 5' splice  
70    site cleavage [8-11].

71       In addition to pre-mRNA splicing, CoSMoS and other colocalization approaches  
72    have been used to study many other multistep biochemical processes including  
73    transcription, translation, DNA replication, and actin filament branching [12-18]. In  
74    general, colocalization experiments involve observation of the binding and release of

75 fluorescent molecules from a surface-tethered substrate. Often this is enabled by the use  
76 of spectrally distinguishable fluorophores (e.g., Cy3 and Cy5), which can be individually  
77 excited and detected [15]. This has allowed multiple fluorescent species to be followed  
78 simultaneously, providing unique insights into biomolecular assembly and disassembly  
79 pathways. Early work on the *S. cerevisiae* (yeast) splicing machinery revealed that  
80 spliceosomes assemble on pre-mRNA in a partially ordered pathway with multiple  
81 reversible steps, potentially identifying points of regulation [19, 20]. Critically, these  
82 experiments also revealed quantitative kinetic information about several discrete steps in  
83 splicing—something which was not possible using earlier approaches such as native gel  
84 electrophoresis of cellular splicing extracts.

85 In this article, we discuss and compare statistical methods that are used to obtain  
86 the fit parameters associated with CoSMoS data of spliceosome assembly. We also  
87 introduce the A GATHering of Analyses (AGATHA) software package that we have  
88 developed to facilitate maximum likelihood fitting of single-molecule data and its statistical  
89 analysis. **We illustrate the use of AGATHA in fitting data related to assembly of splicing**  
90 **factors on RNAs; however, these maximum likelihood methods are generally useful and**  
91 **can be used to analyze single molecule data originating from many different types of**  
92 **experiments beyond pre-mRNA splicing.**

## 93 **2. Example Data and Initial Analysis**

### 94 **2.1. RNA Binding Dynamics of a Yeast Splicing Factor**

95 In order to demonstrate the methods used in statistical analysis of binding times  
96 obtained from single-molecule experiments, we will use two recently published data sets  
97 describing the binding of the yeast splicing factor branchpoint bridging protein (BBP) to

98 pre-mRNA substrates containing or lacking the branch site (BS) [21]. In these  
99 experiments, Larson *et. al* showed that the presence of a BS promotes longer binding of  
100 a fluorescently-tagged BBP molecule to a surface-immobilized RNA. **CoSMoS**  
101 **experiments were performed using a custom built, micromirror TIRF microscope that in**  
102 **which the laser excitation beams enter and exit through the objective.** The workflow for  
103 constructing this microscope has already been published [22]. Pre-mRNAs, labeled with  
104 a red laser-excited Cy5 fluorophore, were first immobilized on a functionalized glass slide.  
105 Whole cell extract containing BBP protein labeled with a green-laser excited Dy549  
106 fluorophore was then added. This experimental set-up for two color CoSMoS is  
107 schematically illustrated in **Figure 1A**. Individual fluorophores were visualized as discrete  
108 spots of intensity, allowing the locations of the RNA and splicing factors to be determined.  
109 Images were then recorded from the camera over time, creating movies of “red”  
110 immobilized RNAs and “green” dynamic BBP proteins. Detailed descriptions of the  
111 experimental set-up and data collection can be found elsewhere [19, 21-26].

## 112 **2.2. Obtaining a List of Dwell Times from Movies of Single Molecules**

113 In the above experiments with BBP, the fluorescence signal from the surface  
114 tethered pre-mRNAs was then used to define Areas Of Interest (AOIs). AOIs were then  
115 mapped from the >635 nm field of view (FOV) corresponding to the “red” pre-mRNA  
116 locations to the <635 nm FOV in which the “green” BBP was imaged [25]. This was then  
117 followed by pixel intensity integration over each AOI, which produced a BBP fluorescence  
118 intensity trajectory at each pre-mRNA location (**Figure 1B**). In this example, the peaks in  
119 fluorescence intensity were identified by changes in signal that exceeded a threshold  
120 value of  $3.2\sigma_s$ , where  $\sigma_s$  represents the baseline noise of the fluorescence trajectory. In

121 effect, the association/dissociation of BBP on an individual RNA corresponds to the  
122 appearance/disappearance of fluorescence peaks from the AOI. The details about  
123 mapping and spot discrimination methods that can be used to obtain the fluorescence  
124 intensity trajectories has been previously described [25].

125 Often a single AOI will show multiple binding events (*cf. Figure 1B*), and each  
126 binding event is characterized by its own binding or dwell time. The dwell times observed  
127 will depend on the biochemical properties of the system studied. For example, inspection  
128 of individual fluorescence trajectories of BBP binding to a pre-mRNA containing a BS  
129 reveals both short and long events (**Figure 1B**). However, when a pre-mRNA lacks a  
130 BS, fluorescence trajectories of BBP binding reveal primarily short events (**Figure 1C**).  
131 This is expected since BBP should most strongly associate with RNAs containing the 5'-  
132 UACUAAC-3' BS sequence [27].

### 133 **2.3. Plotting the Single-Molecule Data as a Distribution of Dwell Times**

134 A single CoSMoS experiment can yield hundreds of dwell times derived from many  
135 different binding events occurring on many different molecules. It is often beneficial to first  
136 plot the dwell time distribution as a probability density (PD) histogram. **In this method,**  
137 **dwell times are first binned, and the population in each bin (  $N_{bin}$ ) is then divided by the**  
138 **product of the bin width (w) and total number of events [  $N_{tot}$ ;  $PD = N_{bin}/(w \times N_{tot})$  ].** The  
139 probability density histograms of dwell times for BBP on RNAs with or without a BS are  
140 compared in **Figure 1D**. The dwell time distribution for BBP binding on RNA that lacks a  
141 BS (dark green) is narrower (shifted towards shorter dwell times) than that obtained from  
142 BBP binding to RNA containing a BS (light green). **This arises due to the scarcity of long-**

143 lived binding events in the absence of the BS. The simplest binding mechanism of BBP  
144 on pre-mRNA (R) without a BS can be described as a single-step process:



145 In contrast, the broader distribution of BBP dwell times on the wild-type RNA could be  
146 due to the presence of two or more populations of BBP-RNA complexes.

147 A more quantitative and theoretical analysis of the dwell time distributions can  
148 provide additional information about kinetic features of the BBP-RNA complexes. The  
149 probability density function (PDF) for the lifetime in an individual state can be described  
150 as an exponential distribution [28]. For mechanisms with multiple states, the probability  
151 density function is the sum of the exponential distributions [28]. A general expression for  
152 PDF with  $k$  states can be written as:

$$PDF(t) = \sum_{i=1}^k \frac{a_i}{\tau_i} e^{-\frac{t}{\tau_i}} \quad \text{for } t > 0 \quad (2)$$

153 where  $\tau_i$ , and  $a_i$ , are the time constant and relative amplitude of the  $i^{th}$  state respectively,  
154 such that  $a_i$  satisfies the constraint  $\sum a_i = 1$ . It is of significant interest to know the  
155 characteristic time constants,  $\tau_i$ , for each complex as they provide information about the  
156 interconversion of the complexes and their relative kinetic stabilities. The values of these  
157 time constants can be extracted by fitting an appropriate equation to the measured data  
158 as discussed below.

### 159 **3. Methods for Fitting Distributions of Dwell Times**

#### 160 **3.1. Obtaining the Fit Parameters and Associated Errors**

161 The method of least squares is frequently used to estimate the best fit parameters.  
162 Although this approach is straightforward and powerful, it can have its pitfalls if not used

163 carefully [29-32]. This is particularly apparent when used to fit data which are not normally  
164 distributed. An alternative approach is the Maximum Likelihood (ML) estimation [33, 34].  
165 For a sufficiently large dataset, different methods should ideally yield the same estimates  
166 for the fit parameters. However, in practice, the extracted fit parameters can often depend  
167 on the chosen method. This will be illustrated in **Section 3.3** by comparing the fit results  
168 obtained from two independent methods. For simplicity, we will focus the discussion  
169 below on fitting and error estimates of kinetic parameters using the ML approach since it  
170 is likely less familiar to most biochemists.

171 Using Equation (2), the probability density for observing the first data point,  $t_1$ ,  
172 reads as

$$PDF(t_1) = \sum_{i=1}^k \frac{a_i}{\tau_i} e^{-\frac{t_1}{\tau_i}} \quad (3)$$

173  
174 As the measurement of one dwell time is independent of any other dwell time observation  
175 within an experiment, the probability density for observing all *then* measured data points,  
176  $t_1, t_2, \dots$  and  $t_n$  can be written as a product of the individual probability densities. This total  
177 probability density defines the likelihood function ( $Lik(\tau_i, a_i)$ ):

$$Lik(\tau_i, a_i) = \prod_{j=1}^n \left[ \sum_{i=1}^k \frac{a_i}{\tau_i} e^{-\frac{t_j}{\tau_i}} \right] \quad (4)$$

178 In other words, the likelihood function characterizes the probability to observe a particular  
 179 set of dwell time values obtained from an experiment. Maximizing the function,  $Lik(\tau_i, a_i)$ ,  
 180 with respect to the parameters  $\tau_i$ , and  $a_i$  will make the observed data most probable.  
 181 Hence, the values of  $\tau_i$  and  $a_i$  that yield a global maximum of  $Lik(\tau_i, a_i)$ , are the best fit  
 182 parameters of the PDF to the experimentally observed distribution.

183 It is important to note that the experimental conditions set limits on the measured  
 184 dwell times ( $t$ ),  $t_m \leq t \leq t_x$ , such that nothing shorter than  $t_m$  can be measured in an  
 185 experiment of duration  $t_x$ . The parameter  $t_m$  is often limited by the camera frame rate.  
 186 These constraints on the dwell times calls for a conditional PDF instead of Equation (2),  
 187 which can be defined as

$$PDF(t) = \frac{a}{\left( e^{-\frac{t_m}{\tau}} - e^{-\frac{t_x}{\tau}} \right)} \left( \frac{e^{-\frac{t}{\tau}}}{\tau} \right), \text{ where } a = 1. \quad (5)$$

188 Similarly, one could obtain the conditional PDF for bi-exponential distribution,

$$PDF(t) = \left[ a_1 \left( e^{-\frac{t_m}{\tau_1}} - e^{-\frac{t_x}{\tau_1}} \right) + a_2 \left( e^{-\frac{t_m}{\tau_2}} - e^{-\frac{t_x}{\tau_2}} \right) \right]^{-1} \left( \frac{a_1}{\tau_1} e^{-\frac{t}{\tau_1}} + \frac{a_2}{\tau_2} e^{-\frac{t}{\tau_2}} \right), \quad (6)$$

189 with  $a_1 + a_2 = 1$ .

190 To obtain the best fit of Equation (5) to the dwell time distribution of BBP on RNA  
 191 without a BS (**Figure 1D**), we maximize the logarithmic likelihood function:

$$L(\tau) = \ln (Lik(\tau)) = -n \ln \left[ e^{-\frac{t_m}{\tau}} - e^{-\frac{t_x}{\tau}} \right] - n \ln (\tau) + \sum_{j=1}^n \left( -\frac{t_j}{\tau} \right). \quad (7)$$

192 Optimizing the product of the probabilities (Equation 4) is often computationally inefficient  
 193 since this product can yield a very small number. With increasing number of data points,

194 this product can run out of precision very quickly due to the floating-point arithmetic used  
195 by computers. Therefore, it is better to maximize the log of the likelihood function as it  
196 converts the product of the individual probability densities to summation and preserves  
197 the fitting results.

198 **Figure 2A** shows the plot between  $L(\tau)$  vs  $\tau$  in which  $L(\tau)$  gets a maximum value of -  
199 909.6 at  $\tau_{max} = 8.6$  s. This  $\tau_{max}$  value is the ML estimate for the fit parameter  $\tau$  for BBP  
200 on RNA without BS. In other words, this parameter indicates that BBP has a characteristic  
201 dwell time of 8.6 s when associating with RNAs lacking a BS sequence.

202 Similarly, one could obtain the ML estimates for  $a_1$ ,  $\tau_1$ ,  $a_2$ , and  $\tau_2$  of the double  
203 exponential PDF [Equation (6)], which is useful for describing the dwell time data set of  
204 BBP on WT RNA. In this case, the more complicated equation is necessary to correctly  
205 fit the appearance of both long and short dwell times in the data set when BBP binds  
206 RNAs containing a BS sequence. A contour plot of the logarithmic likelihood function  $L(\tau_1, \tau_2)$   
207 [corresponding to the double exponential PDF, Equation (6)], is plotted as a function  
208 of  $\tau_1$  and  $\tau_2$  by holding  $a_1$  constant (**Figure 2B**).  $L(\tau_1, \tau_2)$  obtains a maximum value of -  
209 1639.5 at  $\tau_1 = 12.9$  s and  $\tau_2 = 119.3$  s **with the ML estimate for  $a_1 = 0.74$ .**

210 Apart from estimating the optimized fit parameters, it is equally important to  
211 quantify the errors associated with the fit parameters. There are many possible ways to  
212 estimate the errors: a standard approach to assess the standard deviations  
213 corresponding to the parameters estimates is by finding the diagonal elements of the  
214 covariance matrix of  $Lik(\theta_i)$  with respect to fit variables,  $\theta_i$ s [35]. Here, the covariance  
215 matrix can be written as  $C(\theta) = I(\theta)^{-1}$ , where

$$I(\theta_i, \theta_j) = - \left( \frac{\partial^2 \text{lik}(\theta)}{\partial \theta_i \partial \theta_j} \right)_{\theta_{imax}, \theta_{jmax}} \quad (8)$$

216  $\theta_{imax}$ , and  $\theta_{jmax}$  are the ML estimates for  $\theta_i$ , and  $\theta_j$  respectively. For a single exponential  
 217 distribution, it is straightforward from Equations (5) and (8) to obtain an analytical  
 218 expression for standard deviation,  $\sigma \approx \tau_{max}/\sqrt{n}$ , where  $\tau_{max}$  is the ML estimate of  $\tau$ . With  
 219 a total of 288 binding events/dwell times, and  $\tau_{max} = 8.6$  s (data corresponding to **Figure**  
 220 **2A**) the standard deviation turns out to be  $\sim 0.5$  s. It is more difficult to obtain the analytical  
 221 expressions for the standard deviations associated with all parameters of higher order  
 222 exponential distributions. As a result, one can approach these problems using numerical  
 223 analysis.

224 Another way of estimating the error in fit parameters is by finding likelihood  
 225 intervals. The likelihood intervals (*i.e.*, the ranges for the fit parameters) are the values  
 226 most probable within certain neighborhoods around the maxima [29]. For example,  
 227 consider the line,  $L(\tau_{max}) - m$  plotted against the likelihood curve. The points of  
 228 intersection of these curves,  $\tau_{low}$  and  $\tau_{high}$ , will provide a good estimate for the uncertainty  
 229 in  $\tau_{max}$  (**Figure 2A**). The error estimate, in this particular case, depends solely on the  
 230 value of  $m$ . The likelihood intervals for  $m = 0.5$ , and  $m = 2$  correspond to one and two  
 231 standard deviation limits respectively [35]. For higher order exponential distributions, a  
 232 similar procedure can be employed by estimating the error on one parameter while  
 233 keeping the other parameters constant. Likelihood intervals estimates for  $a_1$ ,  $\tau_1$  and  $\tau_2$  are  
 234 shown in **Table 1** for a distribution containing two exponential terms. Likelihood intervals  
 235 estimates are relatively easy to obtain for a single exponential fit but can become  
 236 laborious with increasing numbers of variables.

237 In many cases, the statistical method of bootstrapping is advantageous over the  
238 aforementioned methods in estimating the errors of the fit parameters [36]. Bootstrapping  
239 is a resampling method in which a new data set is generated from the observed data by  
240 random sampling, with the new and original data sets being of the same size. Ideally, this  
241 resampling method preserves the actual distribution of the parameters present in the  
242 observed data set. An example of the bootstrap analysis is illustrated in **Figure 2C**, where  
243 1000 data sets were simulated from the dwell times for BBP on RNA without a BS. The  
244 ML estimates for  $\tau$  were obtained for all 1000 data sets. The distribution of ML estimates  
245 for  $\tau$  was analyzed by plotting a probability density histogram and then fitting to a  
246 Gaussian distribution. The Gaussian fit yields a mean value of 8.6 s and standard  
247 deviation of 0.7 s for  $\tau$ , which are comparable to the ML estimate and 0.5-unit likelihood  
248 intervals (**Figure 2A**). In a similar fashion, one could obtain the uncertainty in the  
249 estimates for a large number of parameters in a fit. A direct comparison of the error  
250 estimates for fit parameters obtained from the likelihood intervals, and the bootstrap  
251 analysis can be found in **Table 1**.

252 **3.2. Determining the Goodness of the Fit**

253 Although ML is a powerful technique, care should be taken in assessing the  
254 goodness of the fit to the unbinned data. This can be done by using statistical tests such  
255 as the likelihood ratio or Akaike Information Criterion (AIC) for model selection based on  
256 the likelihoods [37, 38]. For example, a log likelihood ratio test can identify if the dwell  
257 time distribution for BBP association with WT RNA is better described by single or double  
258 exponential PDFs. The MATLAB function `lratiotest` efficiently implements this procedure  
259 and, in this example, results in rejection of the model based on a single exponential PDF.

260 For fitting of data sets with unknown kinetic features, it is often advisable to begin fitting  
261 to a single exponential PDF. The log likelihood ratio test or AIC can then be used to test  
262 if the simplest model is sufficient or if more complicated PDFs are needed to model the  
263 data. **Figure 2D** shows good agreements between the data and the fit curves for BBP  
264 dwell times on RNAs with and without a BS.

265 Critically, it is **important to consider** the histogram binning since one could easily  
266 bias the fit if the histogram is not binned properly. For example, we created a histogram  
267 with six bins of equal width (100 s each) for the dwell time data set of BBP binding to WT  
268 RNA along with the curve obtained using a ML fit of the unbinned data (**Figure 3A**). It is  
269 evident that the ML fit curve (red) deviates significantly from the equally binned histogram  
270 as well as the curve obtained from least squares fitting of the bin centers (blue line and  
271 black points). To correct this, one can construct an unequally binned histogram with  
272 narrow bin widths for shorter intervals. We have plotted the same ML curve along with  
273 unequally binned histograms of the same data set in **Figures 3B** and **C**. The agreement  
274 between the ML fit and the histogram gets better with increasing number of unequal bins.

### 275 **3.3. Comparison Between Maximum Likelihood and Least Square Fitting**

276 The data plotted in **Figure 3** also illustrate a potential pitfall of least squares fitting  
277 of dwell time distributions. In this case, **the least squares fits were obtained using the**  
278 **curve fitting application of MATLAB (Table 2)**. With least squares fitting, it is possible to  
279 obtain ill-defined fit parameters with large standard deviations despite having reasonable  
280  $R^2$  or adjusted  $R^2$  values. In this case, the least squares fitting is improved by increasing  
281 the number of bins and by using variable bin sizes. If the bin number is large, the least  
282 squares predictions for the parameters approach those obtained by ML estimates

283 (compare parameters in **Table 1** vs. **Table 2**). However, the least squares method results  
284 in broader confidence intervals as compared to the ML error estimates.

285 Additionally, least square fits can be highly sensitive to user inputs for upper and  
286 lower bounds for the fit coefficients as well as sample size. To see the effect of the latter,  
287 we simulated data sets of different sizes with  $a_1 = 0.75$ ,  $\tau_1 = 10.0$  s, and  $\tau_2 = 100.0$  s. As  
288 sample size increases, ML estimates gets very close to the input parameters with  
289 narrower confidence intervals (**Table 3**). However, increasing the number of bins with  
290 these large data sets does result in overestimated values of  $\tau_2$  in least squares fits (**Table**  
291 **3**). This can be attributed to the fact that the least squares method is very sensitive to  
292 outliers, assumes the variables to be independent, and the error to be normal. In cases  
293 where error terms are not normal, the confidence intervals of the least square estimates  
294 are not reliable [24-26]. In our simulation, maximum likelihood outperforms the least  
295 squares method for typical “single molecule”-sized data sets of 100-1000 data points.

296 **4. Use of AGATHA Software for ML Fitting**

297 Here, we introduce "AGATHA" (A GATHering of Analyses), a MATLAB-based  
298 software package that provides tools for the analysis of the dwell times obtained from  
299 CoSMoS experiments (<https://github.com/hoskinslab/AGATHA>). AGATHA includes a  
300 number of subprograms including those for ML analysis (Plotting Histogram), identifying  
301 patterns of signal appearance (Sequential Arrival, Simultaneous Arrival, and Short  
302 Counter), photobleaching analysis (Counting Photobleaching Steps), and data  
303 visualization (Two Color Plot). These programs are accessed via the AGATHA GUI  
304 (**Figure 4**). The Sequential Arrival and Simultaneous Arrival programs are useful for  
305 deducing pathways of signal appearance and disappearance in three color CoSMoS

306 experiments (i.e., determining pathways of biomolecular assembly or disassembly [15]).  
307 These programs classify binding events into various categories depending upon times of  
308 signal appearance or disappearance. The Counting Photobleaching Steps program  
309 counts the number of bleaching steps present in a fluorescence intensity trace by fitting  
310 the data to a step function. This is useful for counting the number of fluorophores  
311 (biomolecules) present in a molecular assembly. Instruction manuals for each of these  
312 programs are found in their respective GUIs. Here, we restrict ourselves to the Plotting  
313 Histogram program as the others are beyond the scope of this article. We also note that  
314 Woody *et. al* have independently developed a similar program, MEMLET (MATLAB  
315 Enabled Maximum Likelihood Estimate Tools), that utilizes the ML approach to fit data by  
316 providing a variety of general or user defined PDFs [34].

#### 317 **4.1. Plotting Histograms**

318 The Plotting Histogram program (PH) facilitates plotting of dwell time data using  
319 various methods for bin size selection as well as ML fitting of the unbinned data. PH  
320 calculates the appropriate number of bins from the chosen method (described below) and  
321 also can remove empty bins by combining neighboring bins. Along with the histogram, it  
322 displays the error in the counting statistics of each bin center by calculating the binomial  
323 distribution variance,  $\sigma_{bin}^2$ , as,  $\sigma_{bin} = \sqrt{nP(1 - P)}$ , where  $n$  is the total number of the data  
324 points, and  $P$  is the probability of the binding event [39]. Finally, it returns the fit  
325 parameters and associated standard deviations by using ML and bootstrap analysis.  
326 AGATHA simplifies ML data analysis by requiring the user to supply the relevant inputs  
327 to entry widgets in the PH GUI (**Figure 5**, numbers 1-7). Fitting results are also displayed

328 in widgets once the program has been run (**Figure 5**, numbers 8 and 9). Below we  
329 describe data entry and use of each of the widgets in the PH GUI.

330 **4.2. Instructions for Using the Plotting Histogram Program**

331 **1-Mode:** In this widget, the user either instructs the software to automatically calculate the  
332 number of bins plotted in a histogram (Automatic) or the user can manually input the bin  
333 edges in increasing order (Manual).

334

335 **2- Histogram:** When Automatic is selected in widget **1**, the user then selects one or more  
336 of the listed methods for calculating the number of bins in the histogram.

337       Sturges: According to the Sturges rule, the number of the bins for a histogram are  
338       estimated based on the range of the given data. This calculates the number of  
339       bins,  $m$ , as  $m = (1 + \log_2(n))$ , where  $n$  is the total number of data points [28, 40].  
340       It will perform poorly if the number of data points is less than 30 and the points are  
341       not normally distributed [41]. As dwell times often follow an exponential distribution  
342       (similar to **Figure 3A**), this method may fail to show an appropriate trend in the  
343       data.

344       Freedman-Diaconis: This method is less sensitive to outliers in a given data, and  
345       might be more suitable for data with heavy-tailed distributions [42]. It uses a bin  
346       width,  $h$ , as  $h = IQR(X) / (n)^{1/3}$ , where  $X$  is the dwell time data,  $n$  is number of data  
347       points, and  $IQR$  is the interquartile range of  $X$ .

348       Scott: This method works better if the data is mostly normally distributed. However,  
349       this rule is appropriate for other distributions as well. It calculates bin width,  $h$ , as

350  $h = 3.5 * \sigma_X / (n)^{1/3}$ , where  $\sigma_X$  is the standard deviation of the data set  $X$ , and  $n$  is

351 number of data points [43].

352 Middle: This method make use of all three methods mentioned above, then

353 choses the middle (median) value for bin numbers.

354 Optimal: An optimization principle is used to minimize the expected least squares

355 loss function between the histogram and an unknown underlying density function

356 [43]. The optimal bin width,  $h^*$ , is obtained as a minimizer of the formula,

357  $(2M - V)/h^2$ , where  $M$  and  $V$  are mean and variance of the data points across bins

358 with a width  $h$ . Optimal number of bins,  $m$ , are calculated as,  $m = (\max(X) - \min$

359  $(X))/h^*$ , where  $\max(X)$ and  $\min(X)$ are the maximum and minimum value of the

360 given data set  $X$ . In our experience, this method is frequently used for plotting

361 dwell time distributions obtained from CoSMoS experiments.

362 All: This selects all of the above methods and runs them independently.

363 **3- Events:** In this widget, the user specifies whether or not the dwell time data is reported

364 in units of time or camera frames.

365

366 **4-Time Units and Intervals:** The time units (seconds or milliseconds) are selected within

367 this widget as well as the interval type from the drop-down menu. AGATHA uses input

368 interval files generated by the GLIMPSE and IMSCROLL programs (available at

369 [https://github.com/gelles-brandeis/CoSMoS\\_Analysis](https://github.com/gelles-brandeis/CoSMoS_Analysis)) [25]. In these programs the dwell

370 times are classified as different types of intervals, each assigned an integer value

371 between -3 and +3. Details about event classification have been previously described [25]  
372 and depend on whether or not the binding the event has been observed in its entirety as  
373 well as whether or not binding events or times between binding events are being  
374 analyzed.

375

376 **5-Function:** PH is equipped with single, double and triple exponential probability  
377 distributions for fitting the measured data. These functions are labelled as Expfallone\_mx1,  
378 Expfalltwo\_mx1, and Expfallthree\_mx1, respectively. PH currently includes equations for  
379 processing up to third order PDFs but can be expanded to higher distributions if needed.

380

381 **6- Input PH Parameters:** The user should enter the experimentally-constrained times Tx  
382 (length of the experiment) and Tm (minimum time that can be resolved by the experiment)  
383 along with a number for Nboot (number of datasets to be simulated for bootstrap analysis)  
384 which is the same as the number of iterations of bootstrap analysis). For example,  
385 Nboot=1000 was used for **Figure 2C**. For single exponential distributions, the user should  
386 enter an initial estimate for Tau [  $\tau$  in Equation (5)]. For bi-exponential PDFs, the user  
387 gives initial guesses for Tau1, Tau2, and ap. **The input value ap is converted to  $a_1 = 1/(1 + ap^2)$  before maximizing the log likelihood in order to constrain  $a_1$  between 0 and 1.**  
388 Similarly, for tri-exponential distribution fit parameters are extended to Tau1, Tau2, Tau3,  
389 ap1 and ap2, and the  $a_1, a_2$ , and  $a_3$  are deduced using equations  $a_1 = 1/(1 + ap1^2), a_2 =$   
390  $(1 - a_1)/(1 + ap2^2)$ , and  $a_1 + a_2 + a_3 = 1$ . If the initial guesses are far off, the program  
391 may crash and fail to find a solution. In which case, new values can be chosen and the  
392 analysis rerun.

394 **7-Update:** Clicking the update button will ask the user to select the intervals file to be  
395 analyzed and to create an output folder for the results.

396 **8-Output Fitting:** The ML estimates for the fit parameters are returned here.

397 **9-Output Bootstrap data:** The mean and standard deviation of the fit parameter values  
398 are displayed after bootstrap analysis. The histograms before and after the fitting will be  
399 saved in the same directory with the same name as the input interval file. The program  
400 also saves the bootstrap results for all the fitting parameters.

401 **5. Conclusion**

402 Programs such as AGATHA and MEMLET facilitate ML fitting of complex single  
403 molecule data with additional capabilities and options not present in many other software  
404 packages such as the MATLAB DF tool. MATLAB's DF tool application only provides a  
405 single exponential function for fitting and cannot fit probability density distributions for  
406 multiple exponential or user-defined PDFs. Both AGATHA and MEMLET are capable of  
407 fitting data with multi-exponential PDFs and provide estimates and errors for fitting  
408 parameters using ML and bootstrapping techniques. Additionally, MEMLET directly  
409 provides likelihood ratio model testing, allows the user to input any PDF, and can take  
410 text or MATLAB variable files as input. On the other hand, AGATHA is supplemented with  
411 various tools for histogram binning and error calculation. Current versions of AGATHA  
412 require input in IMSCROLL format [21]; however, these types of files can be easily  
413 constructed from any data set.

414 In conclusion, ML fitting of unbinned dwell or binding time data is often preferable  
415 compared to least squares fitting of binned data sets, which can be skewed based on

416 how the histogram has been constructed. Implementation of ML methods in MATLAB  
417 can be laborious. Fortunately, this is greatly simplified by the AGATHA software.

418 **Acknowledgements**

419 We thank Joshua Larson, Margaret Rodgers, and Clarisse van der  
420 Feltz for feedback on the manuscript and Laura Vanderploeg for assistance with figure  
421 artwork. We also thank Larry Friedman for helpful discussions and writing the initial  
422 MATLAB scripts for ML fitting as part of CoSMoS data analysis. This work was supported  
423 by the National Institutes of Health (R01 GM112735 to AAH; R01 GM099752 to AS),  
424 Shaw Scientist and Beckman Young Investigator Awards (to AAH), the National Science  
425 Foundation (CHE-1710182 to AS), and the Computation and Informatics in Biology and  
426 Medicine Training Program (National Library of Medicine training grant 5T15LM007359  
427 to SGFC).

428 **FIGURE LEGENDS:**

429 **Figure 1.** Analysis of single-molecule binding dynamics of BBP on RNA substrates. **(A)**  
430 Cartoon schematic of the CoSMoS experiment described by Larson and Hoskins [21] in  
431 which green-labeled BBP binds to and dissociates from a surface-immobilized, red-  
432 labeled RNA substrate either containing (wild-type, WT) or lacking the BS sequence. **(B)**  
433 Single-molecule fluorescence intensity versus time plot showing multiple BBP binding  
434 events on a single WT RNA molecule. One of such binding event is magnified to highlight  
435 a single BBP dwell time. **(C)** Single-molecule fluorescence intensity versus time plot  
436 showing multiple BBP binding events on a single RNA molecule lacking the BS sequence.  
437 **(D)** Comparison between the probability density histograms of dwell times for BBP on  
438 either the WT RNA or the substrate lacking the BS.

439 **Figure 2.** Fitting and statistical analysis of BBP dwell time histograms. **(A)** The log  
440 likelihood function,  $L(\tau)$ , for BBP binding times on RNAs without a BS is plotted as a  
441 function of parameter  $\tau$ . The  $\tau$  low and high values, where the  $L(\tau_{max}) - 0.5$  line intersects  
442 the  $L(\tau)$  curve, are the 0.5 unit intervals: 8.1 s and 9.1 s. Similarly, the 2 unit limits are 7.6  
443 s and 9.6 s. **(B)** Contour plot of the log likelihood function,  $L(\tau_1, \tau_2)$  versus  $\tau_1$  and  $\tau_2$  for  $a_1$   
444  $= 0.74$ .  $L(\tau_1, \tau_2)$  corresponds to the double exponential PDF with dwell times of BBP on  
445 WT RNA. **(C)** Probability density histogram of the ML estimates of  $\tau$  that are obtained  
446 from 1000 random samples ( $N_{boot}=1000$ ) of the dwell time dataset for BBP on RNA  
447 lacking a BS via bootstrapping. The histogram was fit with a Gaussian distribution to  
448 obtain a mean value,  $\mu = 8.6$  s, and the standard deviation,  $\sigma = 0.7$  s. **(D)** Probability  
449 density histograms of the dwell times for BBP are fit with either a single (RNA without BS,  
450 black) or double exponential (WT RNA, red) PDFs. Fit parameters and their respective  
451 error estimates for both data sets are given in **Table 1**.

452 **Figure 3.** Bin size-dependent comparison between ML and least squares fits of dwell time  
453 distributions. The probability density histograms for the dwell times of BBP on WT RNA  
454 with **(A)** 6, equally-sized bin widths, **(B)** 6, variably-sized bin widths, and **(C)** 9, variably  
455 sized bin widths. Lines represent the fits to the bin centers (black points) using least  
456 squares methods (blue) or fits of the unbinned data using ML methods (red). For both  
457 methods, the fit parameters and their corresponding confidence intervals are given in  
458 **Tables 1 and 2**.

459 **Figure 4.** Screenshot of the startup screen for AGATHA software, a collection of  
460 programs designed to expedite analysis of dwell times and fluorescence intensity  
461 trajectories obtained from CoSMoS experiments.

462 **Figure 5.** Screenshot of the Plotting Histogram GUI. Red numbers indicate widgets which  
463 require user input, and blue numbers indicate locations of the fitted parameters output. In  
464 addition, this program also outputs various histograms which are saved in a user-  
465 specified folder.

466

## 467 REFERENCES

468 [1] T.W. Nilsen, The spliceosome: the most complex macromolecular machine in the  
469 cell?, *Bioessays* 25(12) (2003) 1147-1149.

470 [2] M.C. Wahl, C.L. Will, R. Lührmann, The spliceosome: design principles of a dynamic  
471 RNP machine, *Cell* 136(4) (2009) 701-718.

472 [3] W. Chen, M.J. Moore, The spliceosome: disorder and dynamics defined, *Current  
473 Opinion in Structural Biology* 24 (2014) 141-149.

474 [4] S.M. Fica, K. Nagai, Cryo-electron microscopy snapshots of the spliceosome:  
475 structural insights into a dynamic ribonucleoprotein machine, *Nature Structural &  
476 Molecular Biology* 24(10) (2017) 791.

477 [5] Y. Shi, Mechanistic insights into precursor messenger RNA splicing by the  
478 spliceosome, *Nature Reviews Molecular Cell Biology* 18(11) (2017) 655.

479 [6] S.M. Berget, C. Moore, P.A. Sharp, Spliced segments at the 5' terminus of adenovirus  
480 2 late mRNA, *Proceedings of the National Academy of Sciences* 74(8) (1977) 3171-3175.

481 [7] L.T. Chow, R.E. Gelinas, T.R. Broker, R.J. Roberts, An amazing sequence  
482 arrangement at the 5' ends of adenovirus 2 messenger RNA, *Cell* 12(1) (1977) 1-8.

483 [8] R. Rauhut, P. Fabrizio, O. Dybkov, K. Hartmuth, V. Pena, A. Chari, V. Kumar, C.-T.  
484 Lee, H. Urlaub, B. Kastner, Molecular architecture of the *Saccharomyces cerevisiae*  
485 activated spliceosome, *Science* (2016) aag1906.

486 [9] R. Krishnan, M.R. Blanco, M.L. Kahlscheuer, J. Abelson, C. Guthrie, N.G. Walter,  
487 Biased Brownian ratcheting leads to pre-mRNA remodeling and capture prior to first-step  
488 splicing, *Nature Structural & Molecular Biology* 20(12) (2013) 1450.

489 [10] C. Yan, R. Wan, R. Bai, G. Huang, Y. Shi, Structure of a yeast activated spliceosome  
490 at 3.5 Å resolution, *Science* 353(6302) (2016) 904-911.

491 [11] D.J. Crawford, A.A. Hoskins, L.J. Friedman, J. Gelles, M.J. Moore, Single-molecule  
492 colocalization FRET evidence that spliceosome activation precedes stable approach of  
493 5' splice site and branch site, *Proceedings of the National Academy of Sciences* (2013)  
494 201219305.

495 [12] S. Ticau, L.J. Friedman, N.A. Ivica, J. Gelles, S.P. Bell, Single-molecule studies of  
496 origin licensing reveal mechanisms ensuring bidirectional helicase loading, *Cell* 161(3)  
497 (2015) 513-525.

498 [13] L.J. Friedman, J. Gelles, Mechanism of transcription initiation at an activator-  
499 dependent promoter defined by single-molecule observation, *Cell* 148(4) (2012) 679-689.

500 [14] B.A. Smith, S.B. Padrick, L.K. Doolittle, K. Daugherty-Clarke, I.R. Corrêa Jr, M.-Q.  
501 Xu, B.L. Goode, M.K. Rosen, J. Gelles, Three-color single molecule imaging shows  
502 WASP detachment from Arp2/3 complex triggers actin filament branch formation, *Elife* 2  
503 (2013).

504 [15] J.D. Larson, M.L. Rodgers, A.A. Hoskins, Visualizing cellular machines with  
505 colocalization single molecule microscopy, *Chemical Society Reviews* 43(4) (2014) 1189-  
506 1200.

507 [16] S. Uemura, C.E. Aitken, J. Korlach, B.A. Flusberg, S.W. Turner, J.D. Puglisi, Real-  
508 time tRNA transit on single translating ribosomes at codon resolution, *Nature* 464(7291)  
509 (2010) 1012.

510 [17] C.E. Aitken, J.D. Puglisi, Following the intersubunit conformation of the ribosome  
511 during translation in real time, *Nature Structural & Molecular Biology* 17(7) (2010) 793.

512 [18] G. Zhao, E.S. Gleave, M.H. Lamers, Single-molecule studies contrast ordered DNA  
513 replication with stochastic translesion synthesis, *eLife* 6 (2017) e32177.

514 [19] A.A. Hoskins, L.J. Friedman, S.S. Gallagher, D.J. Crawford, E.G. Anderson, R.  
515 Wombacher, N. Ramirez, V.W. Cornish, J. Gelles, M.J. Moore, Ordered and dynamic  
516 assembly of single spliceosomes, *Science* 331(6022) (2011) 1289-1295.

517 [20] I. Shcherbakova, A.A. Hoskins, L.J. Friedman, V. Serebrov, I.R. Corrêa Jr, M.-Q. Xu,  
518 J. Gelles, M.J. Moore, Alternative spliceosome assembly pathways revealed by single-  
519 molecule fluorescence microscopy, *Cell Reports* 5(1) (2013) 151-165.

520 [21] J.D. Larson, A.A. Hoskins, Dynamics and consequences of spliceosome E complex  
521 formation, *eLife* 6 (2017) e27592.

522 [22] J. Larson, M. Kirk, E.A. Drier, W. O'brien, J.F. MacKay, L.J. Friedman, A.A. Hoskins,  
523 Design and construction of a multiwavelength, micromirror total internal reflectance  
524 fluorescence microscope, *Nature Protocols* 9(10) (2014) 2317.

525 [23] E.G. Anderson, A.A. Hoskins, Single molecule approaches for studying spliceosome  
526 assembly and catalysis, *Spliceosomal Pre-mRNA Splicing*, Springer2014, pp. 217-241.

527 [24] S. Hansen, M. Rodgers, A. Hoskins, Fluorescent Labeling of Proteins in Whole Cell  
528 Extracts for Single-Molecule Imaging, Methods in Enzymology, Elsevier2016, pp. 83-104.

529 [25] L.J. Friedman, J. Gelles, Multi-wavelength single-molecule fluorescence analysis of  
530 transcription mechanisms, Methods 86 (2015) 27-36.

531 [26] L.J. Friedman, J. Chung, J. Gelles, Viewing dynamic assembly of molecular  
532 complexes by multi-wavelength single-molecule fluorescence, Biophysical Journal 91(3)  
533 (2006) 1023-1031.

534 [27] J.A. Berglund, K. Chua, N. Abovich, R. Reed, M. Rosbash, The splicing factor BBP  
535 interacts specifically with the pre-mRNA branchpoint sequence UACUAAC, Cell 89(5)  
536 (1997) 781-787.

537 [28] D. Colquhoun, A.G. Hawkes, The Principles of Stochastic Interpretation of Ion  
538 Channel Mechanisms, in: B. Sakmann, E. Neher (Eds.), Single Channel Recording,  
539 Plenum Press, New York, 1995, pp. 397-482.

540 [29] K. Pearson, On the systematic fitting of curves to observations and measurements,  
541 Biometrika 1(3) (1902) 265-303.

542 [30] I.J. Myung, Tutorial on maximum likelihood estimation, Journal of Mathematical  
543 Psychology, 47 (2003) 90-100.

544 [31] U. Genschel, W.Q. Meeker, A comparison of maximum likelihood and median-rank  
545 regression for Weibull estimation, Quality Engineering 22(4) (2010) 236-255.

546 [32] D. Gaeuman, C.R. Holt, K. Bunte, Maximum likelihood parameter estimation for fitting  
547 bedload rating curves, Water Resources Research 51(1) (2015) 281-301.

548 [33] M.A. Ra Fisher, On the mathematical foundations of theoretical statistics, Phil. Trans.  
549 R. Soc. Lond. A 222(594-604) (1922) 309-368.

550 [34] M.S. Woody, J.H. Lewis, M.J. Greenberg, Y.E. Goldman, E.M. Ostap, MEMLET: An  
551 easy-to-use tool for data fitting and model comparison using maximum-likelihood  
552 estimation, *Biophysical Journal* 111(2) (2016) 273-282.

553 [35] D. Colquhoun, F.J. Sigworth, Fitting and Statistical Analysis of Single-  
554 Channel Records, in: B. Sakmann, E. Neher (Eds.), *Single Channel Recording*, Plenum  
555 Press, New York, 1995, pp. 483-588.

556 [36] B. Efron, *The jackknife, the bootstrap, and other resampling plans*, Siam1982.

557 [37] S.S. Wilks, The large-sample distribution of the likelihood ratio for testing composite  
558 hypotheses, *The Annals of Mathematical Statistics* 9(1) (1938) 60-62.

559 [38] H. Akaike, A new look at the statistical model identification, *IEEE Transactions on*  
560 *Automatic Control* 19(6) (1974) 716-723.

561 [39] H.D. Young, *Statistical Treatment of Experimental Data*, McGraw Hill Book  
562 Company, Inc., New York, NY (1962).

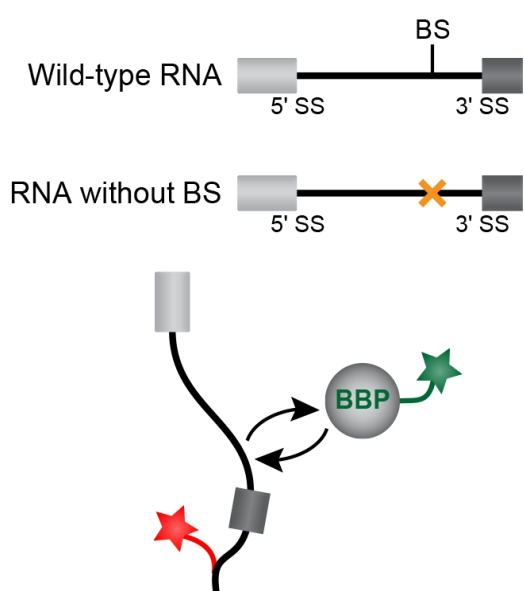
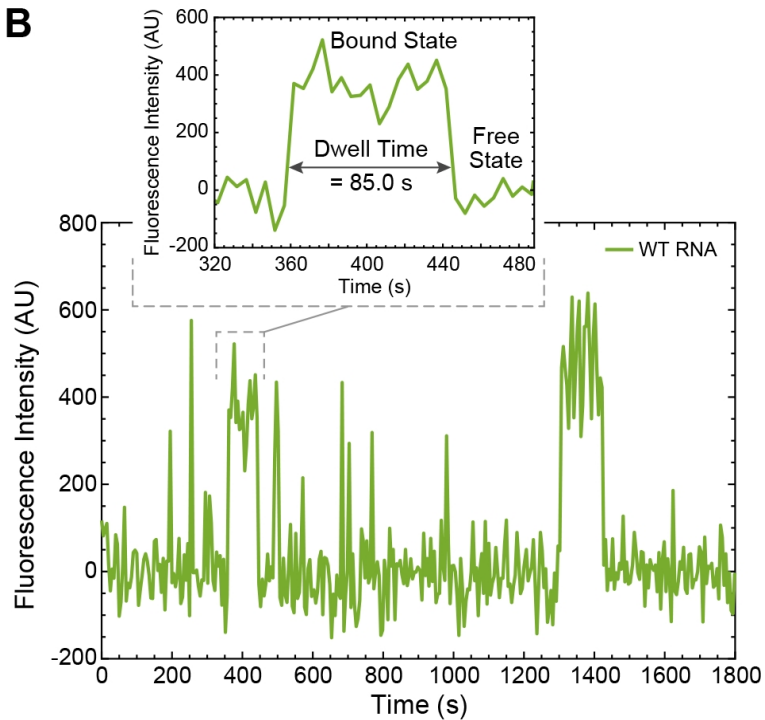
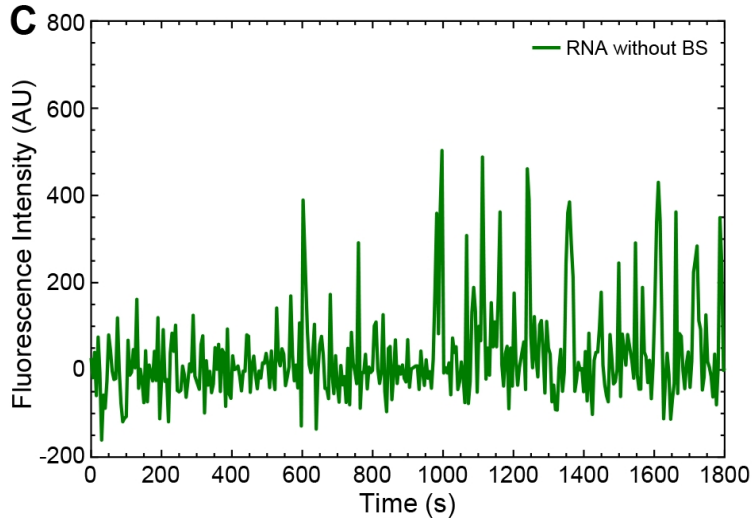
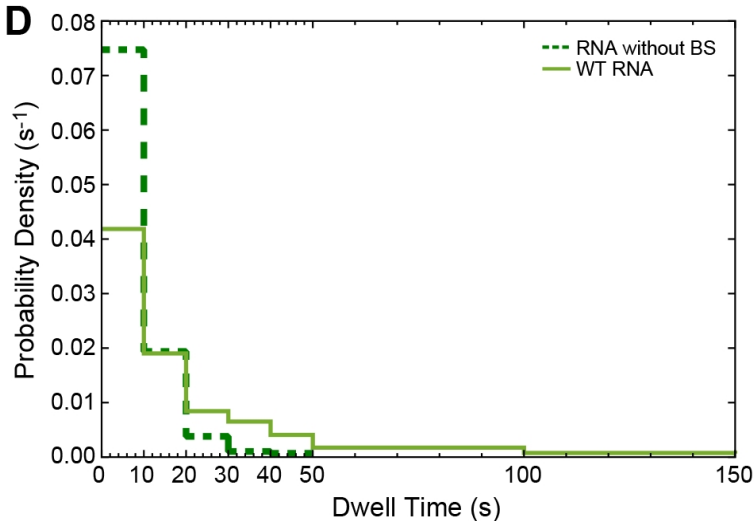
563 [40] H.A. Sturges, The choice of a class interval, *Journal of the American Statistical*  
564 *Association* 21(153) (1926) 65-66.

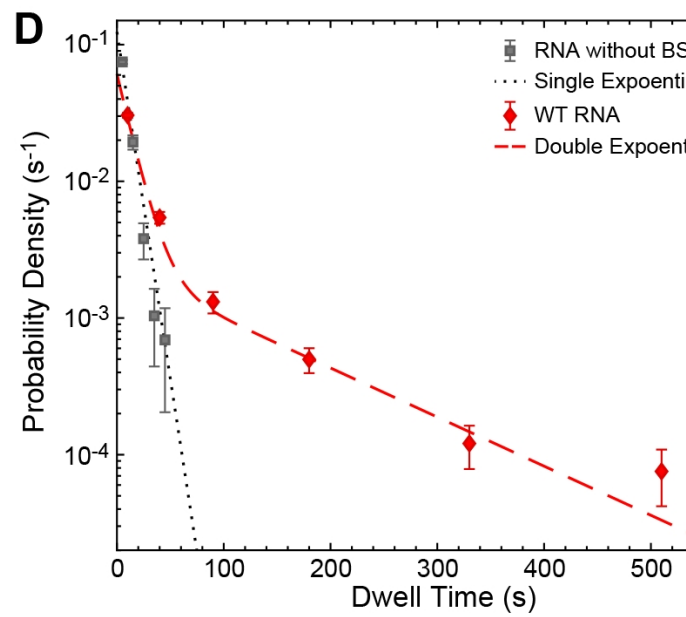
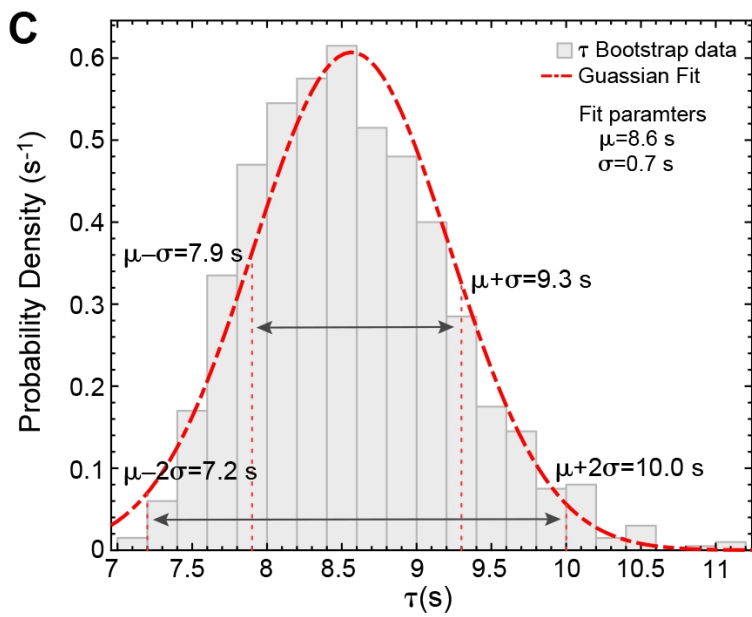
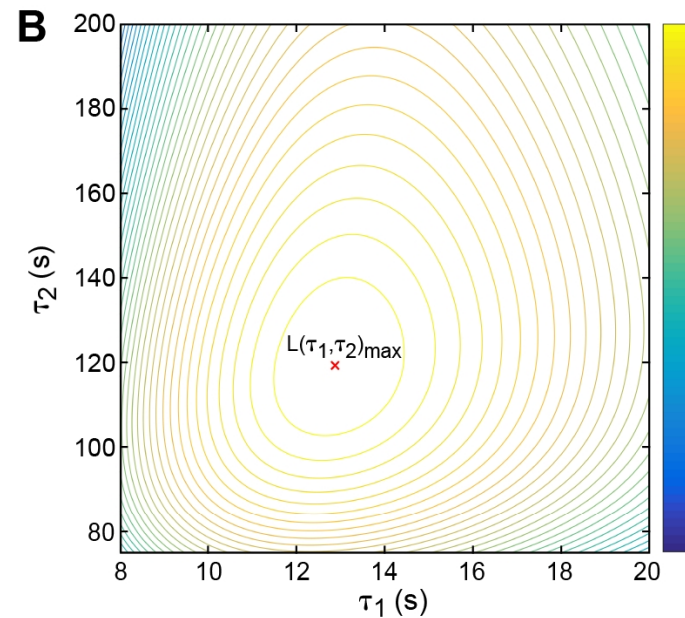
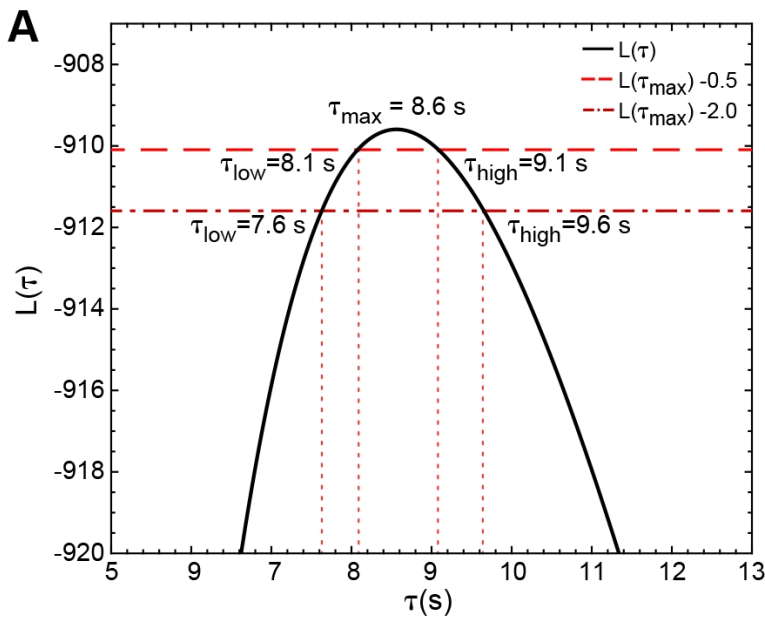
565 [41] R.J. Hyndman, The problem with sturges rule for constructing histograms, (1995).

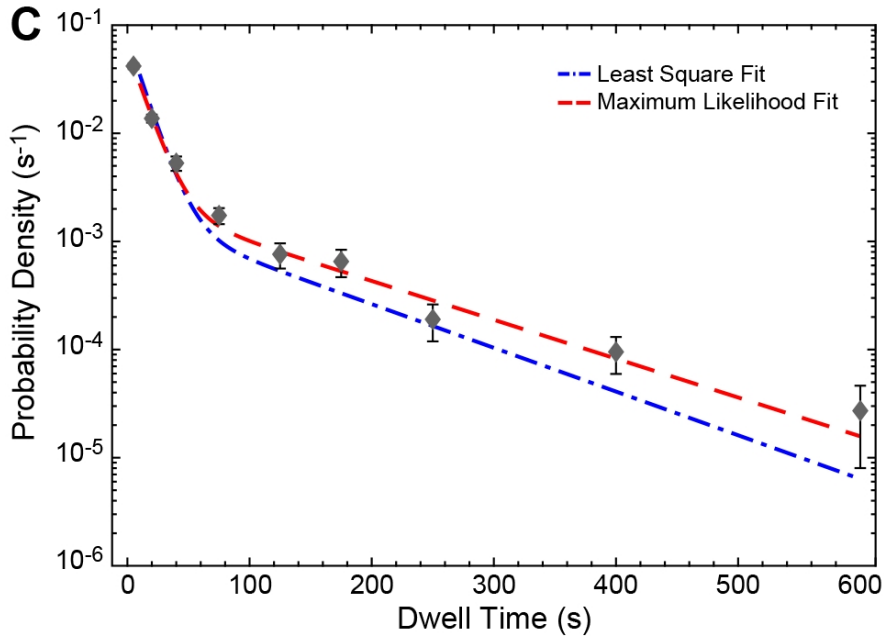
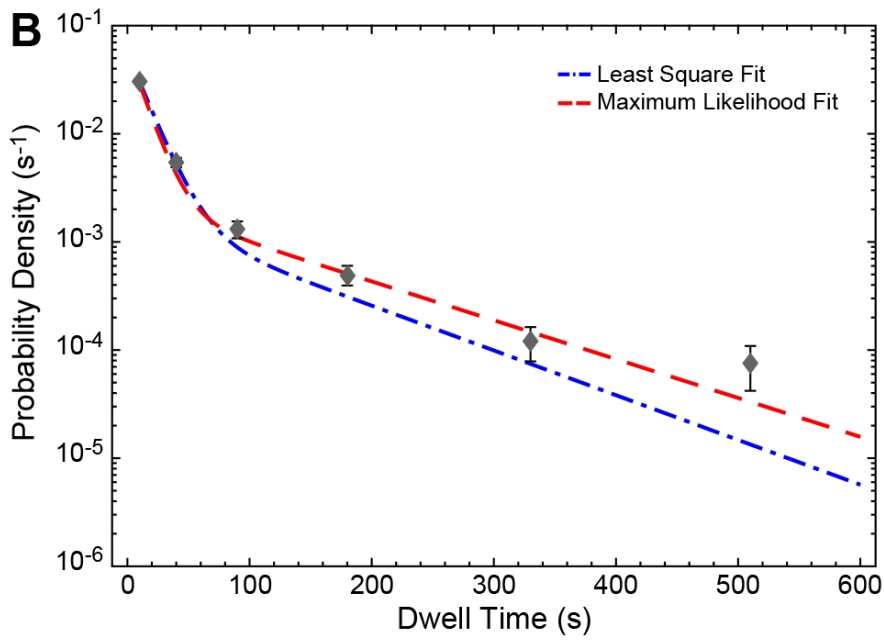
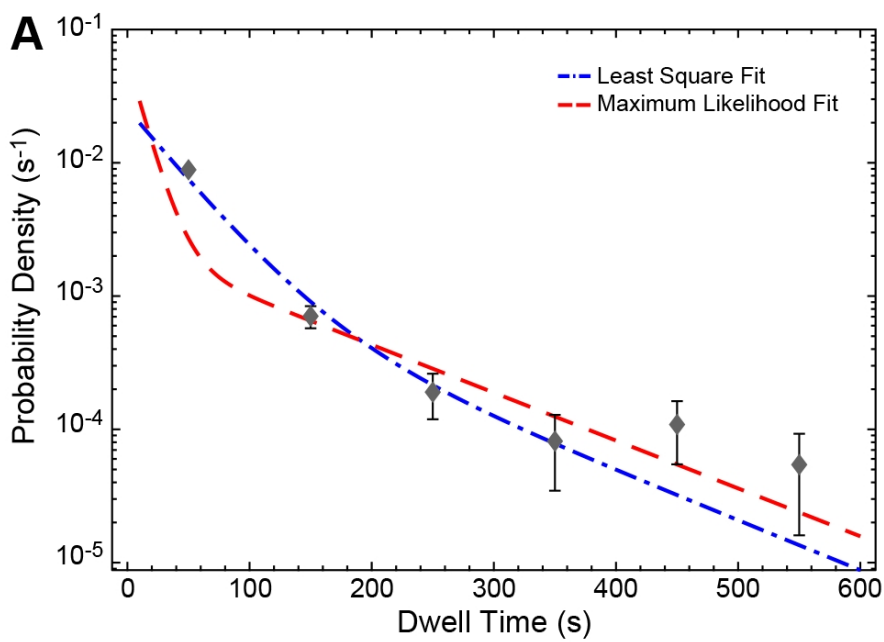
566 [42] D. Freedman, P. Diaconis, On the histogram as a density estimator: L 2 theory,  
567 *Zeitschrift für Wahrscheinlichkeitstheorie und verwandte Gebiete* 57(4) (1981) 453-476.

568 [43] D.W. Scott, On optimal and data-based histograms, *Biometrika* 66(3) (1979) 605-  
569 610.

570

**A****B****C****D**







AGATHA

X



AGATHA

UNIVERSITY OF WISCONSIN-MADISON



Plotting Histogram (Data Fitting)

Sequential Arrival

Two Color Plot

Simultaneous Arrival

Counting Photobleaching Steps

Short Counter

User Manual

GUI\_PLOTTING\_HISTOGRAM

File

1 Mode  Automatic  Manual

2 Method(Histogram)

- Sturges  Freedman-Diaconis
- Scott  Middle value of (St,Fd,Sc)
- Optimal  All

3 Events  Time Duration  Frame Duration

4 Time unit Millisecond Intervals -3

5 Input Parameter

Tx	Tm	Nboot	Tau	Tau1	Function
---	---	---	---	---	Expfallone_mx1
Tau2	Tau3	ap	ap1	ap2	5
---	---	---	---	---	

6 Static Text

7

8 Output fitting

Tau	a1
---	---
Tau1	a2
---	---
Tau2	a3
---	---
Tau3	
---	

9 Output bootstrap data

Tau Mean	Tau1 Mean	Tau2 Mean	Tau3 Mean	a1 Mean	a2 Mean	a3 Mean
---	---	---	---	---	---	---
Std	Std	Std	Std	Std	Std	Std
---	---	---	---	---	---	---

Update User Manual

 Hoskins Lab | University of Wisconsin-Madison

**Table 1.** Comparison between the likelihood intervals and the bootstrap confidence intervals for single and double exponential fits

RNA	PDF Function	Parameter	ML estimate	Likelihood Intervals		Bootstrap Mean	Confidence Intervals	
				m=0.5 68%	m=2 95%		$\sigma$ 68%	2 $\sigma$ 95%
Without BS	Single	$\tau$ (s)	8.6	8.1 9.1 -0.5 0.5	7.6 9.6 -0.9 1.1	8.6	7.9 9.2 -0.7 0.7	7.2 10.0 -1.4 1.4
		$a_1$	0.74	0.70 0.77 -0.03 0.03	0.67 0.79 -0.06 0.06	0.74	0.69 0.78 -0.04 0.04	0.65 0.82 -0.08 0.08
	Double	$\tau_1(s)$	12.9	11.9 13.9 1.0 1.0	10.9 15.2 -2.0 2.3	12.9	11.6 14.2 -1.3 1.3	10.3 15.5 -2.6 2.6
		$\tau_2(s)$	119.4	107.2 133.9 -12.2 14.6	96.5 151.1 -22.9 31.6	120.9	104.4 137.4 -16.5 16.5	87.8 154.0 -33.1 33.1

**Table 1.** Analysis of the double exponential fit to the dwell time distribution for BBP on WT RNA using nonlinear least squares fitting of histogram bin centers.

No. of Bins	Bin Size	Parameter	Non Linear Least Square Fit	Confidence Intervals				R <sup>2</sup> / Adj R <sup>2</sup>	Corresponding Figure
				68%		95%			
6	Equal	$a_1$	0.91	-1.32	3.14	-5.06	6.88		
		$\tau_1(s)$	38.5	-29.2	106.1	-142.6	219.5	0.9465/ 0.9108	3A
		$\tau_2(s)$	116.1	-2399	2631	-6617	6849		
	Variable	$a_1$	0.82	0.74	0.91	0.59	1.06		
		$\tau_1(s)$	15.4	13.5	17.2	10.4	20.3	0.9996/ 0.9994	3B
		$\tau_2(s)$	104.9	22.1	188.0	-116.7	326.5		
9	Variable	$a_1$	0.70	0.65	0.75	0.59	0.81		3C
		$\tau_1(s)$	12.4	11.6	13.2	10.6	14.2	0.9992/ 0.9989	
		$\tau_2(s)$	107.4	69.3	145.5	21.4	193.5		

**Table 3.** Dependence of fitting methods on sample size using simulated data with a double exponential PDF.

Data points	Number of Bins	Bin Size	Parameter	Maximum Likelihood Results*	Nonlinear Least Squares Results*	R <sup>2</sup> /Adj R
100000**	1000	Equal (1s/bin)	$a_1=0.75$	0.74 (0.74 0.74)	0.72 (0.72 0.72)	0.9997/0.9997
			$\tau_1=10$ s	10.9 (10.9 10.9)	10.2 (10.1 10.2)	
			$\tau_2=100$ s	101.8 (100.3 103.1)	123.4 (120.6 126.1)	
10000**	1000	Equal (1s/bin)	$a_1=0.75$	0.75 (0.73 0.76)	0.73 (0.69 0.72)	0.9975/0.9975
			$\tau_1=10$ s	10.9 (10.5 11.3)	10.2 (10.1 10.2)	
			$\tau_2=100$ s	102.7 (107.5 97.1)	122.0 (114.7 130.1)	
10000*	15	Variable	$a_1=0.75$	0.75 (0.73 0.76)	0.76 (0.74 0.79)	0.9999/0.9999
			$\tau_1=10$ s	10.9 (10.5 11.3)	10.8 (10.5 11.1)	
			$\tau_2=100$ s	102.7 (107.5 97.1)	116.0 (80.5 151.5)	
1000	100	Variable	$a_1=0.75$	0.76 (0.72 0.80)	0.73 (0.67 0.81)	0.9951/0.9950
			$\tau_1=10$ s	9.5 (8.3 10.7)	10.4 (10.1 12.8)	
			$\tau_2=100$ s	102.7 (85.7 119.7)	124.8 (88.3 161.4)	
1000	10	Variable	$a_1=0.75$	0.76 (0.72 0.80)	0.76 (0.72 0.80)	0.9999/0.9998
			$\tau_1=10$ s	9.5 (8.3 10.7)	11.08 (10.6 11.6)	
			$\tau_2=100$ s	102.7 (85.7 119.7)	114.4 (60.9 167.9)	
100	10	Variable	$a_1=0.75$	0.79 (0.59 0.99)	0.68 (0.72 1.00)	0.9988/0.9982
			$\tau_1=10$ s	8.9 (3.3 14.5)	6.9 (9.8 14.1)	
			$\tau_2=100$ s	90.7 (17.2 193.2)	50.0 (-3.9 103.9)	

\*Intervals for each fitting method are shown in parentheses.

\*\*Maximum likelihood fitting results obtained using MEMLET software [34]. MEMLET is more efficient at processing large data sets (>10000 data points) than AGATHA software.